

# Low-energy type-II Dirac fermions and spin-polarized topological surface states in transition-metal dichalcogenide NiTe<sub>2</sub>

Barun Ghosh,<sup>1</sup> Debashis Mondal,<sup>2</sup> Chia-Nung Kuo,<sup>3</sup> Chin Shan Lue,<sup>3</sup> Jayita Nayak,<sup>1</sup> Jun Fujii,<sup>2</sup> Ivana Vobornik,<sup>2,\*</sup> Antonio Politano,<sup>4,†</sup> and Amit Agarwal<sup>1,‡</sup>

<sup>1</sup>*Department of Physics, Indian Institute of Technology - Kanpur, Kanpur 208016, India*

<sup>2</sup>*Istituto Officina dei Materiali (IOM)-CNR, Laboratorio TASC, in Area Science Park, S.S.14, Km 163.5, I-34149 Trieste, Italy.*

<sup>3</sup>*Department of Physics, National Cheng Kung University, 1 Ta-Hsueh Road 70101 Tainan, Taiwan*

<sup>4</sup>*Dipartimento di Scienze Fisiche e Chimiche (DSFC), Università dell'Aquila, Via Vetoio 10, I-67100 L'Aquila, Italy*

Using spin- and angle- resolved photoemission spectroscopy (spin-ARPES) together with *ab initio* calculations, we demonstrate the existence of a type-II Dirac semimetal state in NiTe<sub>2</sub>. We show that, unlike PtTe<sub>2</sub>, PtSe<sub>2</sub>, and PdTe<sub>2</sub>, the Dirac node in NiTe<sub>2</sub> is located in close vicinity of the Fermi energy. Additionally, NiTe<sub>2</sub> also hosts a pair of band inversions below the Fermi level along the  $\Gamma - A$  high-symmetry direction, with one of them leading to a Dirac cone in the surface states. The bulk Dirac nodes and the ladder of band inversions in NiTe<sub>2</sub> support unique topological surface states with chiral spin texture over a wide range of energies. Our work paves the way for the exploitation of the low-energy type-II Dirac fermions in NiTe<sub>2</sub> in the fields of spintronics, THz plasmonics and ultrafast optoelectronics.

The discovery of topological semimetals has ushered in a new era of exploration of massless relativistic quasi-particles in crystalline solids[1–4]. These arise as emergent quasi-particles in crystals with linearly dispersing bands in vicinity of a degenerate band crossing point (either accidental or symmetry-enforced) and are protected by crystalline symmetries[5]. Double, triple and quadruple degeneracy of the band crossing leads to topologically protected Weyl[6–14], triple point[15–21] and Dirac fermions[22–30], respectively. In contrast to their high energy counter-parts, these emergent quasi-particles are not protected by Lorentz symmetry, and can also occur in a tilted form, giving rise to type-I and type-II Dirac fermions. Specifically, Na<sub>3</sub>Bi[26, 29] and Cd<sub>3</sub>As<sub>2</sub>[25, 30] are type-I Dirac semimetal (DSM), while the transition-metal dichalcogenides (TMDs) PtTe<sub>2</sub>[31–33], PtSe<sub>2</sub>[34], and PdTe<sub>2</sub>[32, 35, 36] are type-II DSM.

In group X Pd- and Pt- based dichalcogenides, the bulk Dirac node lies deep below the Fermi level ( $\sim 0.6$ ,  $\sim 0.8$  and  $\sim 1.2$  eV in PdTe<sub>2</sub>, PtTe<sub>2</sub>, and PtSe<sub>2</sub>, respectively) [31–36], hindering their successful exploitation in technology. In contrast, NiTe<sub>2</sub> has been predicted to host type-II Dirac fermions in vicinity of the Fermi energy [37]. The so far performed experimental studies on NiTe<sub>2</sub> have primarily focused on its crystal structure, and transport properties while its topological band structure remains unexplored [37–44]. Motivated by this, we explored the electronic band structure of NiTe<sub>2</sub> by means of spin- and angle-resolved photoemission spectroscopy (ARPES) in combination with density functional theory (DFT).

Our spin-resolved ARPES measurements explicitly demonstrate the existence of a pair of type-II Dirac nodes in NiTe<sub>2</sub> along the  $C_3$  rotation axis, lying just above (within 20 meV) the Fermi energy. Additionally, we show that NiTe<sub>2</sub> also hosts a series of inverted band-gaps

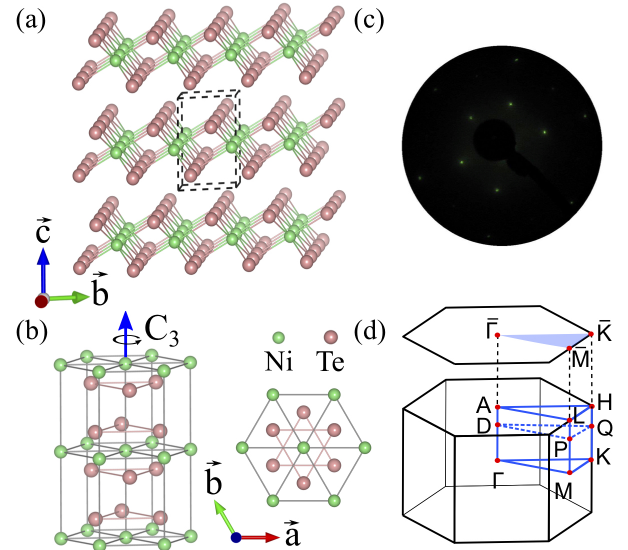


FIG. 1. (a) The side view and (b) hexagonal crystal structure of NiTe<sub>2</sub> with the  $C_3$  rotation axis. Layers of Ni are stuffed between two Te layers. (c) The LEED pattern of (0001)-oriented NiTe<sub>2</sub> single crystals, acquired at a primary electron beam energy of 84 eV, clearly indicates its purity and the six-fold symmetry along along the (001) direction. (d) The bulk and the (001) surface Brillouin zone (BZ) of NiTe<sub>2</sub>.

(IBG). Especially, one of the IBG below the Fermi level supports a Dirac cone in the surface states. Together, the bulk Dirac node and the pair of IBG in NiTe<sub>2</sub> give rise to topological spin-polarized surface states over a wide range of energies. This non-trivial band morphology in NiTe<sub>2</sub> originates primarily from the  $5p$ -orbital manifold of the Te atoms modified by the intra-layer hybridization, trigonal crystal field splitting and spin-orbit coupling.

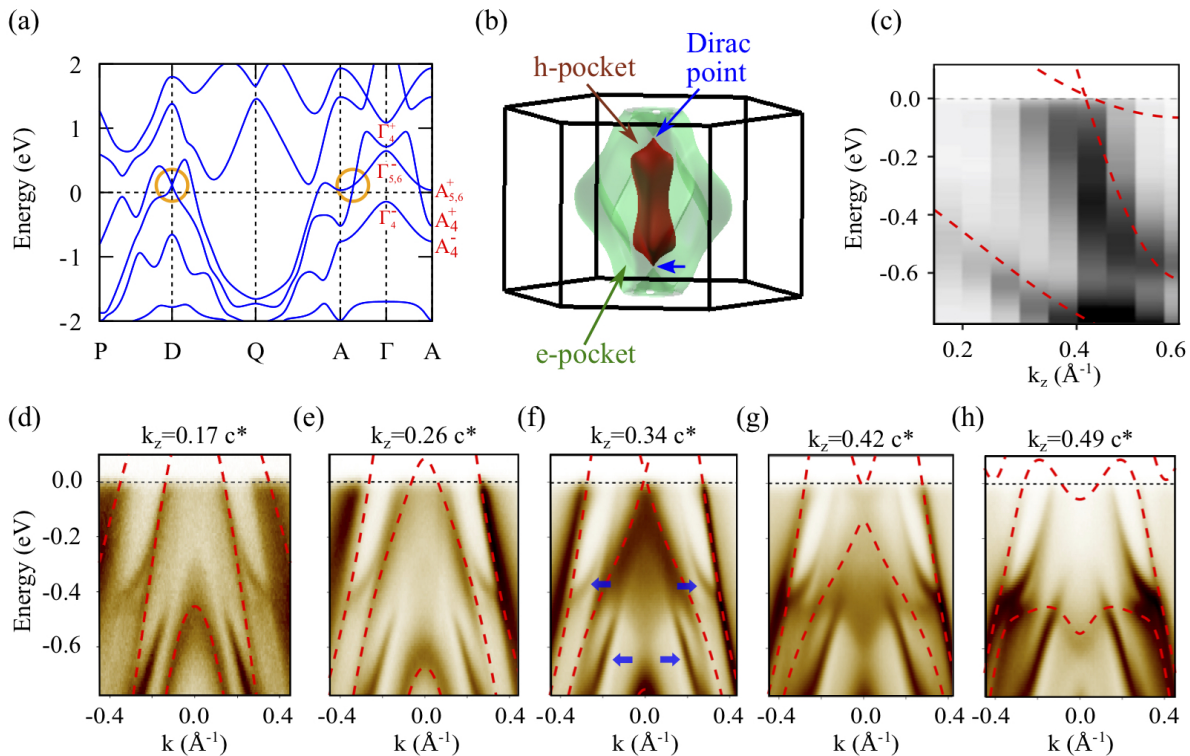


FIG. 2. (a) Band structure of NiTe<sub>2</sub> (including SOC) clearly showing the tilted type-II Dirac node along the  $\Gamma - A$  direction (at D). The irreducible representation of the bands (close to Fermi energy) at the  $\Gamma$  and  $A$  points are also marked. (b) The Fermi surface of NiTe<sub>2</sub> originating from the crossing Dirac bands. The type-II Dirac points appear at the touching points of the electron and hole pockets. (c)  $k_z$  dispersion along  $\Gamma - A$  deduced from the  $h\nu$ -dependent data measured along  $\bar{\Gamma} - \bar{K}$  direction (shown in part in (d-h)); red dashed lines represent the DFT calculations; (d)-(h) The measured band dispersion along the  $\bar{K} - \bar{\Gamma} - \bar{K}$  direction for different  $k_z$  values, with the red dashed lines indicating the bulk DFT band structure. The blue arrows in panel (f) mark the surface states. Data were taken at photon energies of 17, 19, 21, 23 and 25 eV, respectively. Panel (f) corresponding to  $k_z = 0.34 c^*$ , is closest to the location of the Dirac point ( $k_z = 0.35 c^*$  in our DFT calculations). Note that, for matching with the experimental data, we have shifted the DFT band structure downward by 100 meV.

Bulk NiTe<sub>2</sub> crystallizes in the CdI<sub>2</sub> type trigonal structure (space group  $P3m1$ , number 164). It has a layered structure with individual monolayer stacked together via weak van der Waals force. As shown in Fig. 1(a)-(b), each monolayer has three sub-layers, with the central Ni layer being sandwiched between two adjacent Te layers (Ni-Te bond length 2.60 Å). The observation of sharp spots in the low-energy diffraction pattern (LEED) in Fig. 1(c) confirms the high quality of the NiTe<sub>2</sub> crystals cleaved along the (001) direction, along with the presence of six-fold symmetry. Surface cleanliness of the as-cleaved samples was checked by high-resolution electron energy loss spectroscopy and X-ray photoelectron spectroscopy. The details of crystal preparation and characterization, ARPES measurements and DFT calculations are presented in Sec. S1, S2 and S3, of the Supplementary material (SM) [45].

The electronic band structure of NiTe<sub>2</sub> including spin-orbit coupling is shown in Fig. 2(a). It clearly depicts the presence of a pair of tilted band crossings along the

$\Gamma - A$  direction. The presence of inversion and time-reversal symmetry mandates these bands to be doubly degenerate. Furthermore, the  $\Gamma - A$  high-symmetry direction is the invariant subspace of the three fold rotation ( $C_3$ ) symmetry, and a symmetry analysis reveals that the crossing bands have opposite rotation character. This prevents their hybridization, resulting in a pair of gapless quadruply degenerate type-II Dirac points. The type-II nature of the DSM phase is also confirmed by the fact that the Dirac point appears at the touching point of the electron and hole pocket, as highlighted in Fig. 2(b).

Our photon-energy dependent ARPES data, in part presented in Fig. 2(d-h), results in the  $k_z$  dispersion presented in Fig. 2(c). Our experimental results are consistent with the DFT-based bulk band structure calculations. Extrapolating the fitted DFT band structure, we find that the Dirac cone is located just above ( $\sim 20$  meV) the Fermi energy. In contrast to other TMD-based type-II DSMs like PtTe<sub>2</sub>[31–33], PtSe<sub>2</sub>[34], and PdTe<sub>2</sub>[32, 35, 36]. Our attempt to electronically dope

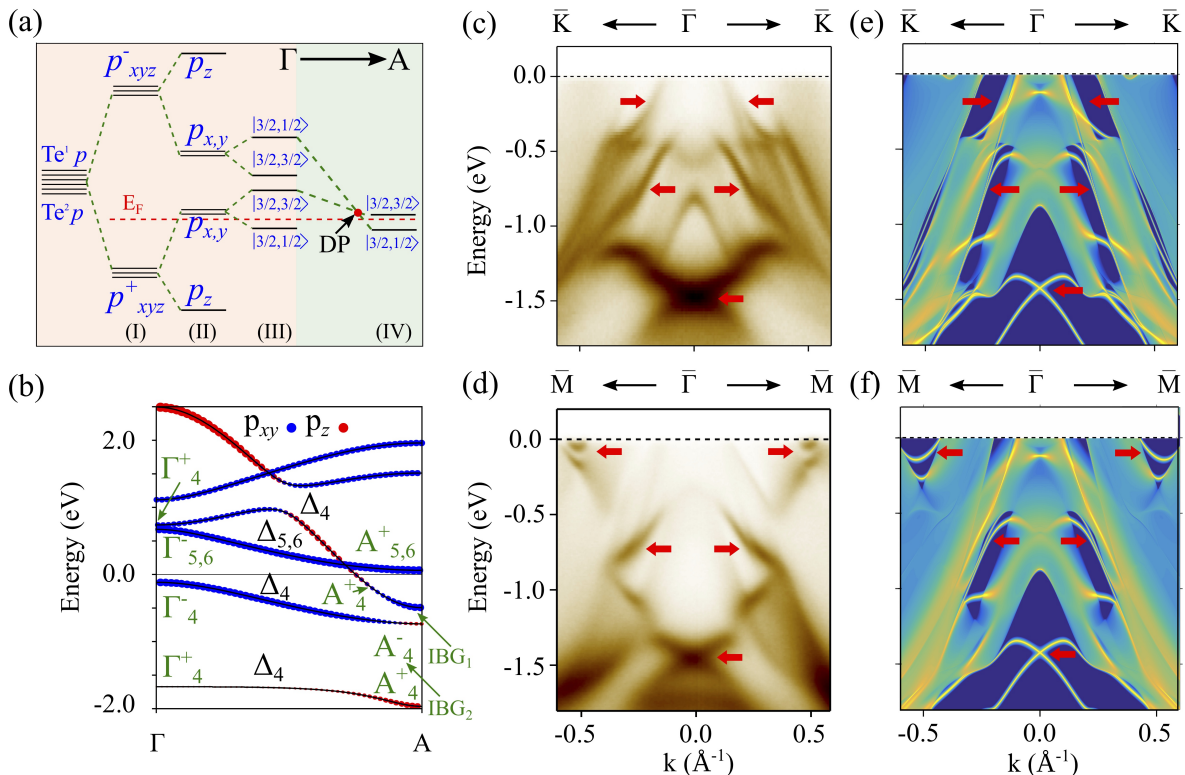


FIG. 3. (a) The evolution of the Te 5p orbitals in the formation of Dirac-cone states in NiTe<sub>2</sub>. Step (I) shows the the creation of bonding and anti-bonding orbitals. Step (II) shows the effect of the strong trigonal crystal field which separates the  $p_z$  orbitals from the  $p_{x,y}$  orbitals. In step (III), we show the splitting of these states into the  $|J, |m_J\rangle$  states in the presence of SOC. In step (IV), we demonstrate the effect of out of plane dispersion and the formation of the Dirac point. (b) The orbital-resolved band structure and various band inversions along the  $\Gamma A$  high-symmetry direction is shown along with the irreducible representations of the bands. In panels (c) and (d) we show the ARPES data (for  $\hbar\nu = 24$  eV) along  $\bar{K} - \bar{\Gamma} - \bar{K}$  and  $\bar{M} - \bar{\Gamma} - \bar{M}$  (for  $\hbar\nu = 30$  eV) directions of the (001) surface BZ, respectively. ARPES results are consistent with the DFT predictions in panels (e) and (f). To match the ARPES results with DFT, we have used a surface potential of  $-0.14$  eV.

the sample via alkali metal (potassium) deposition (see Fig. S6 in the SM [45]), and shift the Fermi energy above the Dirac point, revealed that only the surface states in NiTe<sub>2</sub> are impacted by surface deposition. Bulk doing is needed to shift the bulk bands.

Extended energy range ARPES spectra for the two high-symmetry directions are shown in Fig. 3(c) and (d). These spectra are mainly dominated by the surface states, as seen from the comparison with the calculated band structure in Fig. 3(e) and (f). In order to understand their origin, we note that there are two symmetry inequivalent Te atoms (Te<sup>1</sup> and Te<sup>2</sup>) and a single Ni atom in a unit cell of NiTe<sub>2</sub>. The electronic configuration of Ni is  $3s^2 3d^8$  and that of Te is  $4d^{10} 5p^4$ . We find that similar to other group-X TMDs [32, 46], the Te 5p orbital manifold in NiTe<sub>2</sub>, aided by the interplay between intra-layer hopping, crystal field splitting, and SOC strength, gives rise to most of the bulk Dirac nodes and multiple inverted band-gaps. To highlight this, we show the evolution of the  $p$ -orbital manifold of the Te atoms in Fig. 3(a). To start with (step I in Fig. 3(a)), strong intra-layer hy-

bridization between the Te<sup>1</sup> and Te<sup>2</sup>  $p$  orbitals results in bonding and anti-bonding states. These orbitals are further split (in step II), due to a strong trigonal crystal field generated by the layered crystal structure of NiTe<sub>2</sub>, separating  $p_z$  from the  $p_x, p_y$  orbitals. Inclusion of SOC (step III) further splits the orbitals into  $|J, |m_J\rangle$  states. Step IV of Fig. 3(a) highlights the effect of the dispersion along the  $\Gamma - A$  direction, and the formation of the bulk type-II Dirac point along with multiple band-inversions in the valance band.

The irreducible representation of some of these states at the  $\Gamma$  and  $A$  points and along the  $\Gamma - A$  high-symmetry line is shown in Fig. 3(b). The bulk Dirac point originates from the crossing of the  $\Delta_4$  and  $\Delta_{5,6}$  states along the  $\Gamma - A$  direction. As discussed earlier, the doubly degenerate  $\Delta_4$  and  $\Delta_{5,6}$  bands have opposite rotation characters (+1 and -1, respectively) and, therefore, the Dirac point is protected from gap opening by any perturbation which respects the  $C_3$  symmetry. Additionally, Fig. 3(b) also highlights the existence of a pair of IBGs in the valance band at the  $A$  point. However,

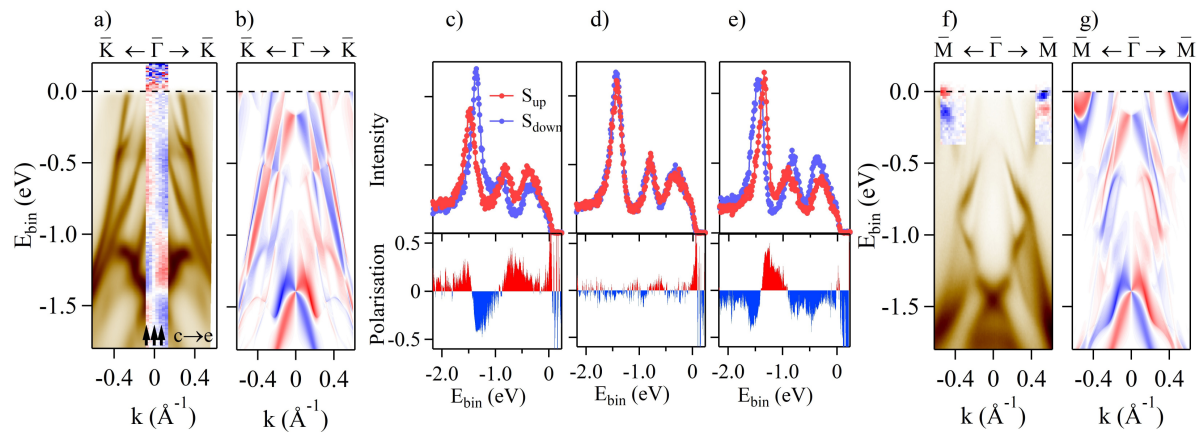


FIG. 4. Measured and calculated spin texture for the bands along  $\bar{\Gamma} - \bar{K}$  (a, b) and  $\bar{\Gamma} - \bar{M}$  (f, g) in the BZ. Experiments were performed in the same conditions as in Figure 3; (c-e) spin-polarized spectra and spin polarization for the points along  $\bar{\Gamma} - \bar{K}$  marked by black arrows in (a); in all figures red/blue indicate positive/negative polarization perpendicular to the high-symmetry direction.  $E_{bin}$  denotes the binding energy.

in comparison to  $\text{PdTe}_2$ , the parity of the crossing bands at the  $A$  point for  $\text{NiTe}_2$  is different and only the lower IBG supports a Dirac node in the surface states. See Sec. S5 in the SM [45] for a more detailed discussion and comparison of the topological band structure and surface states with  $\text{PdTe}_2$ .

The Dirac-like conical crossing in the surface states of  $\text{NiTe}_2$  (at  $-1.4\text{eV}$ ) is evident in the ARPES data taken along the two high-symmetry directions  $\bar{K} - \bar{\Gamma} - \bar{K}$  and  $\bar{M} - \bar{\Gamma} - \bar{M}$  as shown in Figs. 3(c) and (d). The dominant surface bands are indicated by the red arrows. In addition to the Dirac cone, several other surface states are present in  $\text{NiTe}_2$ , owing to several band inversions below and above the Fermi level. Along the  $\bar{M} - \bar{\Gamma} - \bar{M}$  direction, the surface states near the Fermi energy has its origin from a band inversion above the Fermi energy (see Fig. 3(b), and Fig. S3 in SM [45]) and the corresponding surface Dirac cone lies above the Fermi level. While its Dirac-like nature is significantly altered far away from the  $\bar{\Gamma}$  point, we demonstrate its topological origin by displaying its chiral spin texture in Fig. 4. Similar surface states have also been observed in other Te-based TMDs like  $\text{PtTe}_2$  and  $\text{PdTe}_2$ , while they are absent in the Se based compounds like  $\text{PtSe}_2$ . This is a consequence of the avoided band inversion in  $\text{PtSe}_2$  resulting from the reduced interlayer hopping [31, 47].

Since these surface states have a topological origin, we now focus on the spin polarization of the bands using spin-polarized ARPES. In Fig. 4(a) we display the spin-resolved data superimposed directly onto the spin-integrated band structure shown earlier in Fig. 3(c) and (d). The measured spin polarization matches reasonably well with the calculated spin textures reported in Fig. 4(b) and (g). In the present dataset, the spin component is always perpendicular to the dispersion direc-

tion. The most prominent feature in Fig. 4(a)-(b) is the crossover of two opposite spin polarizations of almost equal magnitude for the surface state bands crossing at the  $\bar{\Gamma}$  point at a binding energy of  $\sim -1.4\text{eV}$ . This confirms the helical nature of the spin-momentum locking in vicinity of the surface Dirac point, resulting from the IBG with the  $Z_2 = 1$  topological order. In Fig. 4(c)-(e), we display the spin-polarized spectra and the spin polarization for the points marked by black arrows in Fig. 4(a). The measured polarization perpendicular to  $\bar{\Gamma} - \bar{K}$  reaches almost 50%.

In the case of the bands along  $\bar{M} - \bar{\Gamma} - \bar{M}$  direction of the surface BZ [Fig. 4 (f) and (g)], the polarization was measured for the electron-pocket-like surface states close to the Fermi energy. As discussed previously, although their shape is considerably different than a usual topological surface states, the clear spin polarization demonstrates their topological origin (see Fig. S3 of SM [45]). These indeed appear to be the most prominent spin-polarized features also in the calculated spin polarization perpendicular to the  $\bar{\Gamma} - \bar{M}$  direction. The high values of the measured and calculated spin polarization indicates that  $\text{NiTe}_2$  belongs to the recently identified topological-ladder family of Pt/PdTe<sub>2</sub> [32, 46].

To summarize, we have established the existence of type-II DSM phase in  $\text{NiTe}_2$  single crystals using spin-resolved ARPES measurements in conjunction with DFT-based *ab-initio* calculations. We show that, in contrast to similar class of materials like  $\text{PtTe}_2$ ,  $\text{PdTe}_2$ , and  $\text{PtSe}_2$ , where the Dirac point is buried deep in the valence band, the Dirac point in  $\text{NiTe}_2$  is located in vicinity of the Fermi energy. In addition to the bulk Dirac node, the Te  $p$ -orbital manifold in  $\text{NiTe}_2$  also gives rise to a series of IBGs with non-trivial  $Z_2$  topological orders. Together, these give rise to topological Dirac nodes in the surface

states characterized by the particular spin texture over a wide range of energies. Our findings establish NiTe<sub>2</sub> as a prime candidate for exploration of Dirac fermiology and applications in TMD-based spintronic devices and ultrafast optoelectronics.

### ACKNOWLEDGEMENTS

A.A. acknowledges funding support by Dept. of Science and Technology, Government of India, via DST Grant No. DST/NM/NS/2018/103(G), and from SERB Grant No. CRG/2018/002440. B.G. acknowledges CSIR for senior research fellowship. A. A. and B. G. acknowledges HPC- IIT Kanpur for its computational facilities. This work has been partly performed in the framework of the nanoscience foundry and fine analysis (NFFA-MIUR Italy, Progetti Internazionali) facility.

*Note:* B. G. and D. M. contributed equally to this work as first authors.

---

\* [ivana.vobornik@elettra.trieste.it](mailto:ivana.vobornik@elettra.trieste.it)

† [antonio.politano@iit.it](mailto:antonio.politano@iit.it)

‡ [amitag@iitk.ac.in](mailto:amitag@iitk.ac.in)

- [1] A. Bansil, Hsin Lin, and Tanmoy Das, “Colloquium : Topological band theory,” *Rev. Mod. Phys.* **88**, 021004 (2016).
- [2] M. Z. Hasan and C. L. Kane, “Colloquium: Topological insulators,” *Rev. Mod. Phys.* **82**, 3045–3067 (2010).
- [3] N. P. Armitage, E. J. Mele, and Ashvin Vishwanath, “Weyl and dirac semimetals in three-dimensional solids,” *Rev. Mod. Phys.* **90**, 015001 (2018).
- [4] Desheng Kong and Yi Cui, “Opportunities in chemistry and materials science for topological insulators and their nanostructures,” *Nat. Chem.* **3**, 845 (2011).
- [5] Barry Bradlyn, Jennifer Cano, Zhijun Wang, M. G. Vergniory, C. Felser, R. J. Cava, and B. Andrei Bernevig, “Beyond dirac and weyl fermions: Unconventional quasiparticles in conventional crystals,” *Science* **353**, 6299 (2016).
- [6] Su-Yang Xu, Ilya Belopolski, Nasser Alidoust, Madhab Neupane, Guang Bian, Chenglong Zhang, Raman Sankar, Guoqing Chang, Zhujun Yuan, Chi-Cheng Lee, Shin-Ming Huang, Hao Zheng, Jie Ma, Daniel S. Sanchez, BaoKai Wang, Arun Bansil, Fangcheng Chou, Pavel P. Shibayev, Hsin Lin, Shuang Jia, and M. Zahid Hasan, “Discovery of a weyl fermion semimetal and topological fermi arcs,” *Science* **349**, 613–617 (2015).
- [7] Shin-Ming Huang, Su-Yang Xu, Ilya Belopolski, Chi-Cheng Lee, Guoqing Chang, BaoKai Wang, Nasser Alidoust, Guang Bian, Madhab Neupane, Chenglong Zhang, Shuang Jia, Arun Bansil, Hsin Lin, and M. Zahid Hasan, “A weyl fermion semimetal with surface fermi arcs in the transition metal mononpnictide TaAs class,” *Nature Communications* **6**, 7373 (2015).
- [8] B. Q. Lv, H. M. Weng, B. B. Fu, X. P. Wang, H. Miao, J. Ma, P. Richard, X. C. Huang, L. X. Zhao, G. F. Chen, Z. Fang, X. Dai, T. Qian, and H. Ding, “Experimental discovery of weyl semimetal TaAs,” *Phys. Rev. X* **5**, 031013 (2015).
- [9] Su-Yang Xu, Nasser Alidoust, Ilya Belopolski, Zhujun Yuan, Guang Bian, Tay-Rong Chang, Hao Zheng, Vladimir N. Strocov, Daniel S. Sanchez, Guoqing Chang, Chenglong Zhang, Daixiang Mou, Yun Wu, Lunan Huang, Chi-Cheng Lee, Shin-Ming Huang, BaoKai Wang, Arun Bansil, Horng-Tay Jeng, Titus Neupert, Adam Kaminski, Hsin Lin, Shuang Jia, and M. Zahid Hasan, “Discovery of a weyl fermion state with fermi arcs in niobium arsenide,” *Nature Physics* **11**, 748 (2015).
- [10] Chen Fang, Matthew J. Gilbert, Xi Dai, and B. Andrei Bernevig, “Multi-weyl topological semimetals stabilized by point group symmetry,” *Phys. Rev. Lett.* **108**, 266802 (2012).
- [11] Hongming Weng, Chen Fang, Zhong Fang, B. Andrei Bernevig, and Xi Dai, “Weyl semimetal phase in noncentrosymmetric transition-metal monophosphides,” *Phys. Rev. X* **5**, 011029 (2015).
- [12] Bahadur Singh, Ashutosh Sharma, H. Lin, M. Z. Hasan, R. Prasad, and A. Bansil, “Topological electronic structure and weyl semimetal in the TlBiSe<sub>2</sub> class of semiconductors,” *Phys. Rev. B* **86**, 115208 (2012).
- [13] Tay-Rong Chang, Su-Yang Xu, Daniel S. Sanchez, Wei-Feng Tsai, Shin-Ming Huang, Guoqing Chang, Chuang-Han Hsu, Guang Bian, Ilya Belopolski, Zhi-Ming Yu, Shengyuan A. Yang, Titus Neupert, Horng-Tay Jeng, Hsin Lin, and M. Zahid Hasan, “Type-II symmetry-protected topological dirac semimetals,” *Phys. Rev. Lett.* **119**, 026404 (2017).
- [14] Su-Yang Xu, Nasser Alidoust, Guoqing Chang, Hong Lu, Bahadur Singh, Ilya Belopolski, Daniel S. Sanchez, Xiao Zhang, Guang Bian, Hao Zheng, Marius-Adrian Husanu, Yi Bian, Shin-Ming Huang, Chuang-Han Hsu, Tay-Rong Chang, Horng-Tay Jeng, Arun Bansil, Titus Neupert, Vladimir N. Strocov, Hsin Lin, Shuang Jia, and M. Zahid Hasan, “Discovery of lorentz-violating type II weyl fermions in LaAlGe,” *Science Advances* **3** (2017), 10.1126/sciadv.1603266.
- [15] B. Q. Lv, Z. L. Feng, Q. N. Xu, X. Gao, J. Z. Ma, L. Y. Kong, P. Richard, Y. B. Huang, V. N. Strocov, C. Fang, H. M. Weng, Y. G. Shi, T. Qian, and H. Ding, “Observation of three-component fermions in the topological semimetal molybdenum phosphide,” *Nature* **546**, 627 (2017).
- [16] Wenshuai Gao, Xiangde Zhu, Fawei Zheng, Min Wu, Jinglei Zhang, Chuanying Xi, Ping Zhang, Yuheng Zhang, Ning Hao, Wei Ning, *et al.*, “A possible candidate for triply degenerate point fermions in trigonal layered PtBi<sub>2</sub>,” *Nature communications* **9** (2018).
- [17] Ziming Zhu, Georg W. Winkler, QuanSheng Wu, Ju Li, and Alexey A. Soluyanov, “Triple point topological metals,” *Phys. Rev. X* **6**, 031003 (2016).
- [18] Jiabin Yu, Binghai Yan, and Chao-Xing Liu, “Model hamiltonian and time reversal breaking topological phases of antiferromagnetic half-Heusler materials,” *Phys. Rev. B* **95**, 235158 (2017).
- [19] I. C. Fulga and Ady Stern, “Triple point fermions in a minimal symmetric model,” *Phys. Rev. B* **95**, 241116 (2017).
- [20] Hao Yang, Jiabin Yu, Stuart S. P. Parkin, Claudia Felser, Chao-Xing Liu, and Binghai Yan, “Prediction of triple point fermions in simple half-Heusler topological insulators,” *Phys. Rev. Lett.* **119**, 136401 (2017).

- [21] Jianfeng Wang, Xuelei Sui, Wujun Shi, Jinbo Pan, Shengbai Zhang, Feng Liu, Su-Huai Wei, Qimin Yan, and Bing Huang, “Prediction of ideal topological semimetals with triply degenerate points in the  $\text{NaCu}_3\text{Te}_2$  family,” *Phys. Rev. Lett.* **119**, 256402 (2017).
- [22] S. M. Young, S. Zaheer, J. C. Y. Teo, C. L. Kane, E. J. Mele, and A. M. Rappe, “Dirac semimetal in three dimensions,” *Phys. Rev. Lett.* **108**, 140405 (2012).
- [23] Steve M. Young and Charles L. Kane, “Dirac semimetals in two dimensions,” *Phys. Rev. Lett.* **115**, 126803 (2015).
- [24] Benjamin J. Wieder, Youngkuk Kim, A. M. Rappe, and C. L. Kane, “Double dirac semimetals in three dimensions,” *Phys. Rev. Lett.* **116**, 186402 (2016).
- [25] Z. K. Liu, B. Zhou, Y. Zhang, Z. J. Wang, H. M. Weng, D. Prabhakaran, S.-K. Mo, Z. X. Shen, Z. Fang, X. Dai, Z. Hussain, and Y. L. Chen, “Discovery of a three-dimensional topological dirac semimetal,  $\text{Na}_3\text{Bi}$ ,” *Science* **343**, 864–867 (2014).
- [26] Z. K. Liu, J. Jiang, B. Zhou, Z. J. Wang, Y. Zhang, H. M. Weng, D. Prabhakaran, S.-K. Mo, H. Peng, P. Dudin, T. Kim, M. Hoesch, Z. Fang, X. Dai, Z. X. Shen, D. L. Feng, Z. Hussain, and Y. L. Chen, “A stable three-dimensional topological dirac semimetal  $\text{Cd}_3\text{As}_2$ ,” *Nature Materials* **13**, 677 (2014).
- [27] Madhab Neupane, Su-Yang Xu, Raman Sankar, Nasser Alidoust, Guang Bian, Chang Liu, Ilya Belopolski, Tay-Rong Chang, Horng-Tay Jeng, Hsin Lin, Arun Bansil, Fangcheng Chou, and M. Zahid Hasan, “Observation of a three-dimensional topological dirac semimetal phase in high-mobility  $\text{Cd}_3\text{As}_2$ ,” *Nature Communications* **5**, 3786 (2014).
- [28] Sergey Borisenko, Quinn Gibson, Danil Evtushinsky, Volodymyr Zabolotnyy, Bernd Büchner, and Robert J. Cava, “Experimental realization of a three-dimensional dirac semimetal,” *Phys. Rev. Lett.* **113**, 027603 (2014).
- [29] Zhijun Wang, Yan Sun, Xing-Qiu Chen, Cesare Franchini, Gang Xu, Hongming Weng, Xi Dai, and Zhong Fang, “Dirac semimetal and topological phase transitions in  $\text{A}_3\text{Bi}$  ( $\text{a} = \text{Na, K, Rb}$ ),” *Phys. Rev. B* **85**, 195320 (2012).
- [30] Zhijun Wang, Hongming Weng, Quansheng Wu, Xi Dai, and Zhong Fang, “Three-dimensional dirac semimetal and quantum transport in  $\text{Cd}_3\text{As}_2$ ,” *Phys. Rev. B* **88**, 125427 (2013).
- [31] Mingzhe Yan, Huaqing Huang, Kenan Zhang, Eryin Wang, Wei Yao, Ke Deng, Guoliang Wan, Hongyun Zhang, Masashi Arita, Haitao Yang, Zhe Sun, Hong Yao, Yang Wu, Shoushan Fan, Wenhui Duan, and Shuyun Zhou, “Lorentz-violating type-ii dirac fermions in transition metal dichalcogenide  $\text{PtTe}_2$ ,” *Nature Communications* **8**, 257 (2017).
- [32] M. S. Bahramy, O. J. Clark, B. J. Yang, J. Feng, L. Bawden, J. M. Riley, I. Marković, F. Mazzola, V. Sunko, D. Biswas, S. P. Cooil, M. Jorge, J. W. Wells, M. Leandersson, T. Balasubramanian, J. Fujii, I. Vobornik, J. E. Rault, T. K. Kim, M. Hoesch, K. Okawa, M. Asakawa, T. Sasagawa, T. Eknapakul, W. Meevasana, and P. D. C. King, “Ubiquitous formation of bulk dirac cones and topological surface states from a single orbital manifold in transition-metal dichalcogenides,” *Nature Materials* **17**, 21 EP – (2017).
- [33] Antonio Politano, Gennaro Chiarello, Barun Ghosh, Krishanu Sadhukhan, Chia-Nung Kuo, Chin Shan Lue, Vittorio Pellegrini, and Amit Agarwal, “3d dirac plasmons in the type-ii dirac semimetal  $\text{PtTe}_2$ ,” *Phys. Rev. Lett.* **121**, 086804 (2018).
- [34] Kenan Zhang, Mingzhe Yan, Haoxiong Zhang, Huaqing Huang, Masashi Arita, Zhe Sun, Wenhui Duan, Yang Wu, and Shuyun Zhou, “Experimental evidence for type-ii dirac semimetal in  $\text{PtSe}_2$ ,” *Phys. Rev. B* **96**, 125102 (2017).
- [35] Han-Jin Noh, Jinwon Jeong, En-Jin Cho, Kyo Kim, B. I. Min, and Byeong-Gyu Park, “Experimental realization of type-ii dirac fermions in a  $\text{PdTe}_2$  superconductor,” *Phys. Rev. Lett.* **119**, 016401 (2017).
- [36] Fucong Fei, Xiangyan Bo, Rui Wang, Bin Wu, Juan Jiang, Dongzhi Fu, Ming Gao, Hao Zheng, Yulin Chen, Xuefeng Wang, Haijun Bu, Fengqi Song, Xiangang Wan, Baigeng Wang, and Guanghou Wang, “Nontrivial berry phase and type-ii dirac transport in the layered material  $\text{PdTe}_2$ ,” *Phys. Rev. B* **96**, 041201 (2017).
- [37] Chunqiang Xu, Bin Li, Wenhe Jiao, Wei Zhou, Bin Qian, Raman Sankar, Nikolai D. Zhigadlo, Yanpeng Qi, Dong Qian, Fang-Cheng Chou, and Xiaofeng Xu, “Topological type-ii dirac fermions approaching the fermi level in a transition metal dichalcogenide  $\text{NiTe}_2$ ,” *Chemistry of Materials* **30**, 4823–4830 (2018).
- [38] Enji Uchida and Hisamoto Kondoh, “Magnetic properties of nickel telluride,” *Journal of the Physical Society of Japan* **11**, 21–27 (1956).
- [39] M. Ettenberg, K.L. Komarek, and E. Miller, “Thermodynamic properties of nickel-tellurium alloys,” *Journal of Solid State Chemistry* **1**, 583 – 592 (1970).
- [40] G Y Guo and W Y Liang, “Study of the electronic structures of ni-group metal ditellurides:  $\text{NiTe}_2$ ,  $\text{PdTe}_2$  and  $\text{PtTe}_2$  by the self-consistent LMTO-ASA method,” *Journal of Physics C: Solid State Physics* **19**, 5365–5380 (1986).
- [41] P J Orders, J Liesegang, R C G Leckey, J G Jenkin, and J D Riley, “Angle-resolved photoemission from the valence bands of  $\text{NiTe}_2$ ,  $\text{PdTe}_2$  and  $\text{PtTe}_2$ ,” *Journal of Physics F: Metal Physics* **12**, 2737–2753 (1982).
- [42] Joo Frederico Haas Leandro Monteiro, Mariana Braga Marciniak, Alcione Roberto Jurelo, Ezequiel Costa Siqueira, Fbio Teixeira Dias, and Jorge Luiz Pimentel Jnior, “Synthesis and microstructure of  $\text{NiTe}_2$ ,” *Journal of Crystal Growth* **478**, 129 – 133 (2017).
- [43] Bei Zhao, Weiqi Dang, Yuan Liu, Bo Li, Jia Li, Jun Luo, Zhengwei Zhang, Ruixia Wu, Huifang Ma, Guangzhuang Sun, Yu Huang, Xidong Duan, and Xiangfeng Duan, “Synthetic control of two-dimensional  $\text{NiTe}_2$  single crystals with highly uniform thickness distributions,” *Journal of the American Chemical Society* **140**, 14217–14223 (2018).
- [44] Qianqian Liu, Fucong Fei, Bo Chen, Xiangyan Bo, Boyuan Wei, Shuai Zhang, Minhao Zhang, Faji Xie, Muhammad Naveed, Xiangang Wan, Fengqi Song, and Baigeng Wang, “Nontopological origin of the planar hall effect in the type-ii dirac semimetal  $\text{NiTe}_2$ ,” *Phys. Rev. B* **99**, 155119 (2019).
- [45] Supplementary material detailing 1) Sample preparation and characterization, 2) computational details, 3) ARPES measurements, 4) Topological band inversions and 5) ARPES measurements with potassium doping, is available at <https://bit.ly/2YWzff1o>.
- [46] O J Clark, F Mazzola, I Marković, J M Riley, J Feng, B-J Yang, K Sumida, T Okuda, J Fujii, I Vobornik, T K Kim, K Okawa, T Sasagawa, M S Bahramy, and P D C

- King, “A general route to form topologically-protected surface and bulk dirac fermions along high-symmetry lines,” [Electronic Structure](#) **1**, 014002 (2019).
- [47] O. J. Clark, M. J. Neat, K. Okawa, L. Bawden, I. Marković, F. Mazzola, J. Feng, V. Sunko, J. M. Riley, W. Meevasana, J. Fujii, I. Vobornik, T. K. Kim, M. Hoesch, T. Sasagawa, P. Wahl, M. S. Bahramy, and P. D. C. King, “Fermiology and superconductivity of topological surface states in PdTe<sub>2</sub>,” [Phys. Rev. Lett.](#) **120**, 156401 (2018).